 doi:10.20944/preprints202106.0545.v1

Article

Formulation and characterization of a new injectable bone substitute composed PVA/borax /$CaCO_3$ and Demineralized Bone Matrix

Daniela Medrano-David[1]*, A.M. Lopera-Echavarría[1], Martha E. Londoño[1] and Pedronel Araque-Marín[2,3]

[1] Research group GIBEC, EIA University, Envigado (Colombia); marta.londo@eia.edu.co
[2] Research and Innovation Group in Chemical Formulations, EIA University; pedronel.araque@eia.edu.co
[3] CECOLTEC, Medellín (Colombia); pedronel.araque@eia.edu.co
* Correspondence: daniela.medrano@eia.edu.co

Abstract: The occurrence of bone-related disorders and diseases has increased dramatically in recent years around the world. Demineralized bone matrix (DBM) has been widely used as a bone implant due to its osteoinduction and bioactivity. However, the use of DBM is limited because it is a particulate material, which makes it difficult to manipulate and implant with precision, in addition, these particles are susceptible to migrate to other sites. To address this situation, DBM is commonly incorporated into a variety of carriers. An injectable scaffold has advantages over bone grafts or preformed scaffolds, such as the ability to flow and fill the bone defect. The aim of this research is to develop a DBM carrier with such viscoelastic properties to obtain an injectable bone substitute (IBS). The DBM carrier developed consisted of a PVA/glycerol network cross-linked with borax and reinforced with CaCO3 as a pH neutralizer, porosity generator, and source of Ca. The physicochemical properties were determined by the injectability test, FTIR, SEM, and TGA. Porosity, degradation, bioactivity, possible cytotoxic effect, and proliferation in osteoblasts were also determined. The results show that the developed material has great potential to be used in bone tissue regeneration.

Keywords: Bone tissue regeneration; injectable; bone graft; fracture; osteoblast; bone tissue engineering

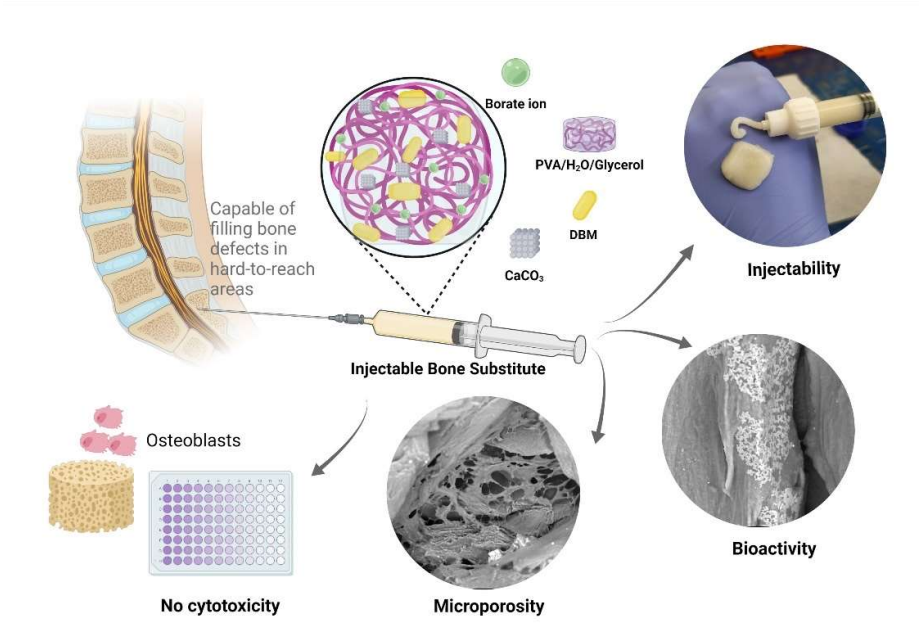

Graphical abstract. Created in https://biorender.com/

Preprints (www.preprints.org) | NOT PEER-REVIEWED | Posted: 22 June 2021 doi:10.20944/preprints202106.0545.v1

1. Introduction

With the increasing number of bone defects in the world, methods to achieve rapid and efficient healing of defective bones are attracting more attention. In particular, injectable bone substitutes (IBS) have been identified as suitable biomaterials for bone regeneration [1]. These materials, unlike solid and preformed scaffolding, allow them to be applied using minimally invasive surgical techniques, reducing intervention time, recovery time, and risk of infection [2]. In addition, IBS facilitates the filling of any irregularly shaped defect and this allows direct contact between the injected material and the surface of the bone tissue to be treated [3]. Injectable hydrogels have attracted much attention, especially because their structures are similar to the extracellular matrix [4] and provide adhesion, proliferation, differentiation and migration of stem cells [5]. In recent years, various injectable hydrogels with good formability and three-dimensional structure have been studied for their application in bone tissue engineering [6]. Although these hydrogels exhibit great potential for promoting bone regeneration, their poor mechanical properties limit their further clinical application [7].

The choice of the most appropriate polymer depends on the biocompatibility, the lack of side effects upon implantation (such as inflammation or allergy), and the physical-chemical properties such as degradation, and reabsorption [8][9]. Polyvinyl alcohol (PVA) has been extensively studied for its biocompatibility, hydrophilic properties, chemical resistance and biochemical properties [10][11]. In addition, it is a non-toxic, water-soluble, biocompatible, biodegradable, and safe polymer for medical use [12]. With a large number of hydroxyl groups in the chain, combined with excellent water retention, PVA is an ideal choice for self-healing hydrogels, which can self-heal after the material has cracked or broken. This self-repairing design not only extends the life of the material but also restores and/or maintains its original performance[13]. Borax-crossed PVA hydrogels have a physical crosslinking network through hydrogen bonds and reversible diol-borate ester [14]. The specific mechanism of the complexity of PVA with borax is as follows: a borax mol is dissociated into 2 mol of borate ions and borate acid as shown in

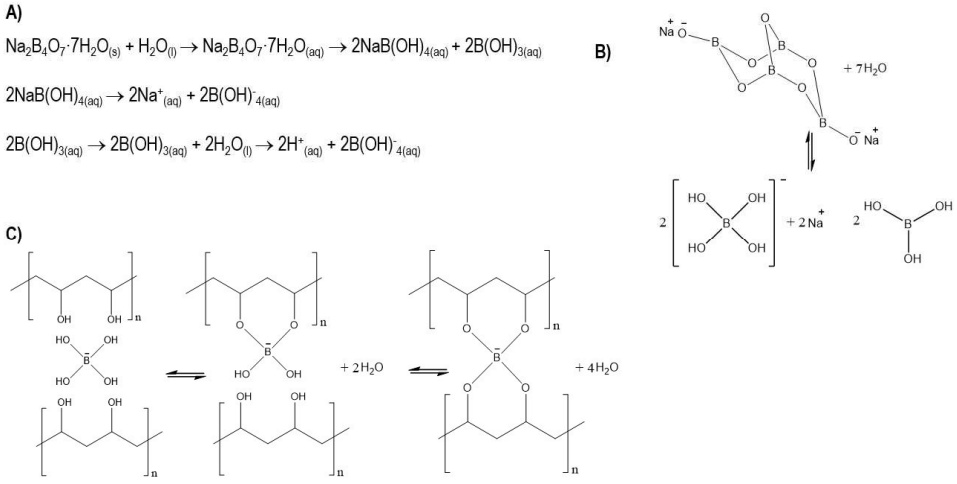

Figure **1**. The complexity mechanism of PVA-borate ions has two balances governed by interaction with hydrogen, monodiol, and didiol complexities [15]. The complex of PVA and Borax in aqueous solutions has been thoroughly studied for several decades [16][17]. Its compatibility with biological environments has been proven and its properties have allowed hydrogels to be considered promising for various applications such as tissue engineering [18], drug release [19], and wound dressing [20]. As a flexible material, the PVA - Borax hydrogel received the attention of this work, as a carrier of DBM because it can form a self-healing hydrogel, which would increase the stability of the injectable system during and after injection.

 doi:10.20944/preprints202106.0545.v1

Recently, through the introduction of bioactive inorganic compounds, many composite hydrogel scaffolds with enhanced mechanical properties have been developed for bone regeneration [21]. DBM is currently still considered a good candidate in clinical practices due to its osteoinductive and osteoconductive properties [22][23][24][25]. For this reason, this research combined the physicochemical properties of borax cross-linked PVA hydrogel with the osteoconductive and osteoinductive properties of DBM to create an injectable bone substitute. In addition, $CaCO_3$ was incorporated to increase osteoconductivity and neutralize pH [26][27][28]. The injectability of the developed materials was evaluated, they were also characterized by FTIR, SEM, and TGA. The porosity was determined by the liquid displacement technique. The in vitro degradation kinetic was determined by the immersion technique in simulated body fluid (SBF), and this fluid was also used for the evaluation of bioactivity, which consists of analyzing the surface of the materials after immersion in SBF, looking for calcium phosphates. Finally, the cytotoxicity of the IBS was evaluated by the MTT assay and the cell proliferation using Alamar Blue Kit.

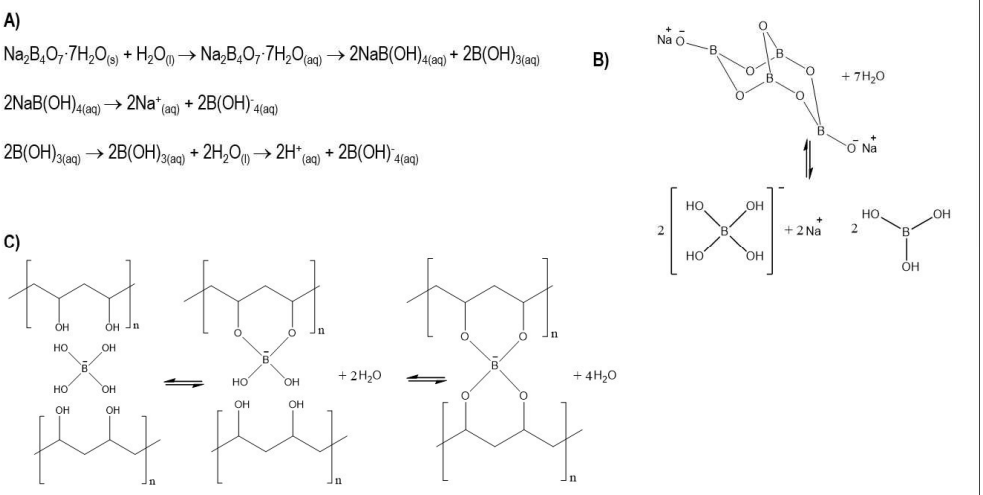

Figure 1. (A) Chemical equations of dissociation of sodium tetraborate (borax) in water. **(B)** Model of dissociation **(C)** Physical-chemistry crosslinking process and complexity balance between PVA chains and borate ions

2. Materials and Methods

2.1 Materials: The demineralized bone matrix (DBM) with particle size between 125 - 300 μm was obtained by the Tissue Bank Foundation, Medellín, Colombia. PVA polyvinyl alcohol [-CH_2CHOH-] n Mw 130,000, 99% hydrolyzed; calcium carbonate [$CaCO_3$]; and borax [$Na_2B_4O_7{\cdot}7H_2O$] were acquired from Sigma Aldrich Co (USA). Glycerol was acquired in JM chemicals (Colombia). For simulated body fluid (SBF) were used: sodium chloride (NaCl), sodium bicarbonate (NaHCO3), potassium chloride (KCl), dipotassium hydrogen phosphate trihydrate ($K_2HPO_4{\cdot}3H_2O$), magnesium chloride hexahydrate ($MgCl_2{\cdot}6H_2O$), hydrochloric acid (HCl), calcium chloride ($CaCl_2$), sodium sulfate (Na_2SO_4), and basic TRIS purchased from Sigma Aldrich Co (USA). All solutions were prepared with Milli-Q Water with an electrical conductivity of approx. 0.18 μS.

Human osteosarcoma osteoblasts (Saos-2 ATCC ® HTB-85 ™ cell line), McCoy's 5A culture medium with bicarbonate, L-glutamine, fetal bovine serum (FBS), and antibiotics (penicillin-streptomycin) were used for the biological evaluation. Phosphate saline buffer (PBS), MTT (Thiazolyl blue tetrazolium bromide) by Thermo Fisher was used for cytotoxicity evaluation and Alamar-Blue Invitrogen from Thermo Fisher for the evaluation of cell proliferation.

2.2. Methods

Preprints (www.preprints.org) | NOT PEER-REVIEWED | Posted: 22 June 2021 doi:10.20944/preprints202106.0545.v1

2.2.1 Injectable Bone substitute preparation: A liquid phase composed of PVA/glycerol solution in a 1/3 ratio and borax 3% were mechanically mixed with a solid phase of DBM and calcium carbonate. Final injectable bone substitute samples were added in syringes for ease of application. The

Table 1 specifies the composition percentages of each sample or formulation.

Table 1. The composition of formulations evaluated in this study.

Approx. weight composition (%)						
Formulation	Powders			Liquids		
	DBM	$CaCO_3$	PVA	Glycerol	Borax	Water
1	26	2	2	6.5	0.5	63
2	25	5	2	6.5	0.5	61
3	24	5	3.6	6.5	0.4	60.5

2.2.2 Injectability

To measure the extrusion force necessary to inject the substitutes, an equal volume (1 mL) of each of the formulations was filled into a 2 mL syringe without a needle, which was fixed vertically and perpendicularly to the clamp in a universal machine. Instron mechanical test machine, model: 3345, at 26 °C with a load cell of 5000 N and a speed of 5 mm/min. Each experiment was repeated three times. This methodology was based on the methodology employed by Dyah Hikmawati and co-authors [29].

$$Injectability\ (\%) = \left(\frac{mass\ extruded\ from\ the\ syringe}{total\ mass\ before\ injectaion}\right) x\ 100\% \quad \textbf{(1)}$$

2.2.3. Physicochemical characterization

Scanning electron microscopy (Phenom ProX Desktop SEM) was used to examine sample morphology and microstructure of the sample, then, by Image J the pore sizes were measured. Using the liquid displacement methodology (hexane) implemented by Rutusmita Mishra et al. the percentage of porosity was measured [30]. Fourier transform infrared ray (FTIR - ATR, Perkin Elmer Spectrum 100) spectroscopy was performed in the range of 4000 – 550 cm^{-1} with the resolution of 4 cm^{-1} to evaluate the binding of all the components of the injectable system. In order to know the thermal behavior of the injectable formulations, a thermogravimetric analyzer, TA Instruments, model TGA Q500 was used. The heating ramp used was 5 °C/min from 30 ° C to 1200 °C under Nitrogen atmosphere.

2.2.4. Degradation

To evaluate the degradation of the injectable bone substitute, samples of the different formulations were immersed in plastic containers containing 5 mL simulated physiological fluid (SBF) at a temperature of 37 °C for periods of 3, 7, 14, 21, and 28 days. The samples were measured for pH (acidity test) and weighed before immersion and on each proposed day of observation (according to ASTM F2900-11, which describes mass loss as a degradation kinetics test for biomedical hydrogels). The test is carried out with the SBF prepared in the Biomaterials laboratory according to the Kokubo protocol [31]. At the end of each proposed period, the samples were frozen and subsequently lyophilized to guarantee that the moisture acquired during the immersion time was eliminated [32]. Weight loss (W_L) was calculated as shown in Eq. (2) where W_0 denotes the initial dry weight of the samples, and W_d represents the weight of the dry samples after the programmed immersion time [33].

$$Weight\ loss\ (\%) = \frac{W0-W}{Wd}\ x\ 100 \quad \textbf{(2)}$$

2.2.5. Bioactivity evaluation

To determine the bioactivity property of IBS, the methodology proposed by Kokubo was used, which requires simulated body fluid (SBF) with pH adjusted to 7.4 to immerse the samples in for a specified time at a temperature of 37 °C. The samples after completing 3, 7, and 14 days of immersion in SBF, were left to dry in a vacuum desiccator at 37 °C temperature, and finally, they were analyzed by means of scanning electron microscopy

Preprints (www.preprints.org) | NOT PEER-REVIEWED | Posted: 22 June 2021 doi:10.20944/preprints202106.0545.v1

(SEM) in order to analyze the surface of the material and identify the possible formation of apatite crystals [31] [34]. The composition of the material formed on the surface was evaluated by means of Energy Dispersive X-ray Spectroscopy (Phenom ProSuite v2.8.0 EDX).

2.2.6. Cell culture

The Saos-2 cell line (ATCC ® HTB-85 ™) human osteosarcoma osteoblasts were grown in McCoy's 5A culture medium reconstituted with 2.2 g/L bicarbonate, 10 mL/L L-glutamine and 10% supplemented with fetal bovine serum (FBS) and 1% antibiotics (penicillin-streptomycin). The culture medium was changed every two or three days and the incubation conditions were 37 °C and 5% CO_2.

2.2.7. MTT assay

During the assay, the medium was removed and replaced by 10 % MTT solution in cell medium; it was then incubated for 4 h at 37 °C and protected from light. After this time, this reagent was removed, and the formazan crystals were dissolved adding 200 µL of DMSO. The MTT reduction was quantified by measuring the light absorbance with a BIO-RAD X Mark microplate reader at a wavelength of 570 nm for 10 sec with orbital motion.

2.2.8 Cell proliferation

The osteoblast monolayer was used for the evaluation of cell proliferation using the Alamar blue kit from Thermo Fisher, which evaluates the mitochondrial ability to reduce resazurin in the fluorescent product resorufin. 50,000 cells/well were seeded in a 96-well dish. Before carrying out the assay, the Alamar Blue medium was prepared by mixing medium with Alamar Blue solution in a ratio of 10:1, after treatment with the formulations for 24, 48, and 72 h, the medium was discarded and replaced by the medium with Alamar Blue. The microplates were incubated at 37 °C for 3 h and the fluorescence was measured using a BIO-RAD X ELISA reader at an excitation wavelength of 535 nm and an emission wavelength of 590 nm. Cell viability was calculated using the ratio between the fluorescence of the treated cells and the fluorescence of the control cells.

2.2.9. Statistical analysis

After testing the normal distribution of the data with the Shapiro-Wilk test, the groups were compared using one-way analysis of variance (ANOVA) and then the post hoc test (Tukey) was used. Significant differences were verified by Student's t-test. Values of $p < 0.05$ were considered statistically significant. All measurements in the different tests were collected at least in triplicate and expressed as mean ± standard deviation (SD). Statistical analysis was performed with Minitab 19 software.

3. Results

3.1. Injectability

Injectable hydrogels are a class of hydrogels that can be extruded through a syringe [35]. The objective of the test is to determine the force necessary to extrude the material through a syringe, as well as the percentage of that injectability using Equation 1. The results are summarized in **Error! Reference source not found.** .

Table 2. Injectability test results

Formulation	Máx. compression load (N)	Injectability (%)
1	50 ± 2	93 ± 1
2	13 ± 1	94 ± 1
3	193 ± 29	59± 19

The injection behavior of formulations 1 and 2 is shown in Figure 2, where the y-axis represents the compression stress (N) exerted by the load cell on the syringe plunger, and the x-axis the displacement made by this same. This figure identifies three relevant events in injection behavior, which are reported by other authors [36][37] and indicated in said figure from left to right as follows:

Preprints (www.preprints.org) | NOT PEER-REVIEWED | Posted: 22 June 2021 doi:10.20944/preprints202106.0545.v1

1. "Overexertion" or "overshoot": initial overstrain is required to overcome hydraulic pressure inside the syringe.

2. Platea or plateau: this area indicates a greater presence of solids, the plateau in this case is wide.

3. Maximum effort at the end of the injection: indicates the point of mechanical resistance, exerted by the plunger against the end of the syringe.

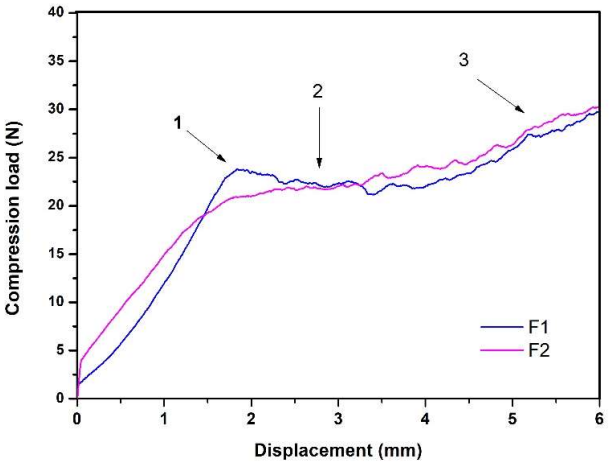

Figure 2. Injectability behavior of formulations 1 and 2.

3.2. Physicochemical characterization

One of the reasons for incorporating calcium carbonate is because this material produces a powerful and prolonged neutralization of acidity, forming $CaCl_2$ and CO_2 [38]**.** In this work, it was also decided to take advantage of the release of CO_2 generated by effervescence [39] that happens when the system is prepared to generate porosity to the material. The results of the liquid displacement test show that F2 has the highest percentage of porosity concerning F1, 53.19 ± 0.01 and 50.8 ± 0.1 respectively. It is important to note that F2 is composed of 5% $CaCO_3$ and F1 is 2%, consequently, it is possible to suggest that as the content of $CaCO_3$ in the system increases, the porosity also increases. The pore sizes obtained by Image J of both injectable formulations were analyzed by ANOVA. It was found that between F1 and F2 there were no statistically significant differences, which suggests that when decreasing the percentage of $CaCO_3$ from 5% to 2%, the pore size does not vary

Preprints (www.preprints.org) | NOT PEER-REVIEWED | Posted: 22 June 2021 doi:10.20944/preprints202106.0545.v1

significantly, however, the percentage of porosity does. Histograms of pore size values are represented in **Error! Reference source not found.**.

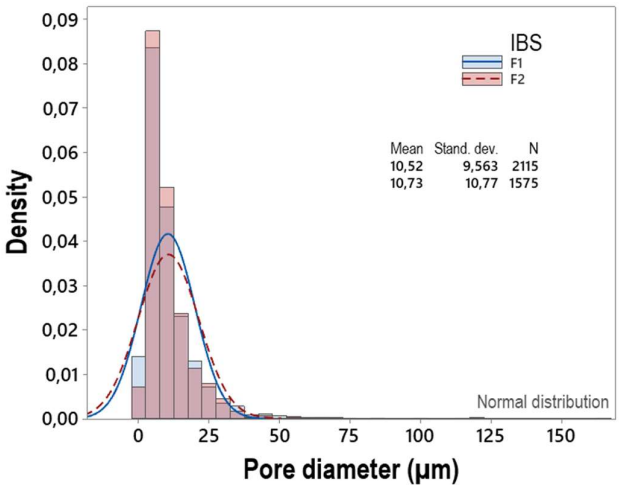

Figure 3. Histogram of pore diameters

Error! Reference source not found. shows the results of the physicochemical characterization of F1 and F2. SEM micrographs show, in all cases, a heterogeneous surface with pores and clusters of cubic morphology, which correspond to calcium carbonate. This was verified by EDS. $CaCO_3$ clusters could provide roughness to the surface of the material, which could favor cell adhesion [40], however, this hypothesis must be verified by a cell adhesion assay for these composite materials.

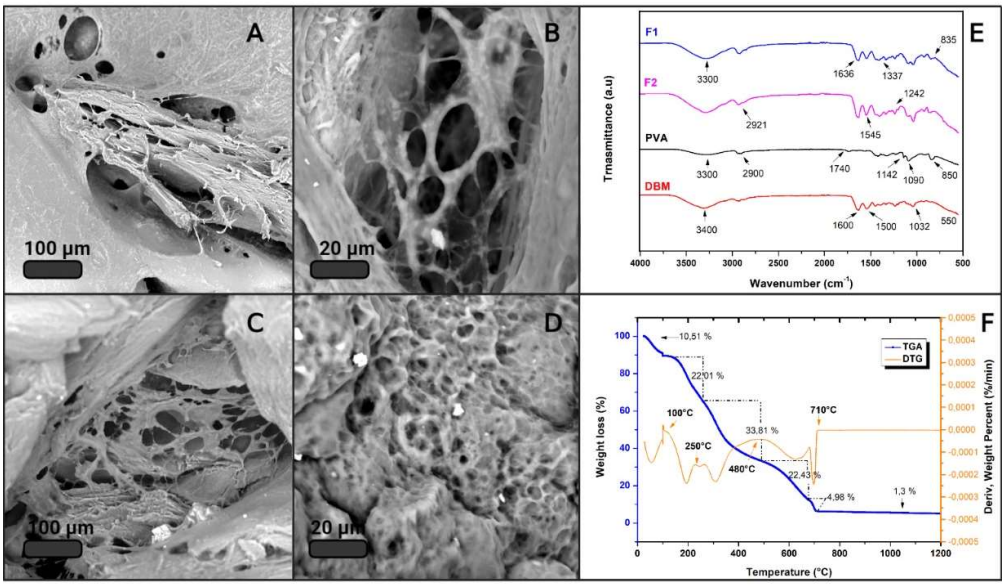

Figure 4. Physicochemical characterization. (A and B) SEM of F1; (C and D) SEM of F2; (E) FTIR spectrum of the main components, F1 and F2; (F) TGA.

An FTIR analysis was performed on main IBS components, to characterize the most representative functional groups of each material, **Error! Reference source not found.**(E) shows the IR spectra of PVA, DBM, F1, and F2. The red spectrum corresponds to the DBM showing a band around 3400 cm^{-1} associated with OH groups. The most representative DBM peaks were identified at 1600 and 1500 cm^{-1}, which are attributed to vibrations of the

 doi:10.20944/preprints202106.0545.v1

amide groups of collagen and other proteins [41]. The band at 1032 cm^{-1} and the beginning of a band at 550 cm^{-1} are associated with the bending mode caused by vibration of phosphate group PO_4^{3-}, confirming the presence of calcium phosphates, a mineral component of bone, which remains as a residual mineral component after demineralization of DBM [42]. The black spectrum corresponding to PVA shows the characteristic bands of polyvinyl alcohol. Around 2900 cm^{-1} there appears a band attributed to the stretching of the C-H alkyl and broadband at 3300 cm^{-1} is typical of the hydroxyl group (free alcohol, OH stretching). A band was also identified around 1090 cm^{-1} and a small one at 1740 cm^{-1} [43] which, according to the literature [44] [45] [46], is mainly attributed to the crystallinity of PVA, related to the carboxyl stretch band (C=O). The band at 1142 cm^{-1} has been used as an evaluation tool for the structure of the semi-crystalline PVA [47]. The spectra of F1 and F2 appear to be an overlap of the spectra of PVA and DBM. It is observed in the two spectra, the broadband at a height of 3300 cm^{-1} that is attributed to moisture absorption and a small one at 1637 cm^{-1} that is attributed to hydroxyl vibrations. The peaks at 2921 cm^{-1}, 1436 cm^{-1}, 1242 cm^{-1}, 1035 cm^{-1} and 8345 cm^{-1} in the broadband can be assigned to the vibrations of CH_2, double bond C=C and C-O respectively [48]. The band at 1042 cm^{-1} is related to an asymmetric P-O stress due to PO_4^{3-}. The vibrations around 1180 cm^{-1} correspond mainly to minerals, in this case, the source of calcium is $CaCO_3$ [49]. The band that appears at 1337 cm^{-1} is due to the O–H bending of the hydroxyl groups that interact with borate ions or forming intermolecular hydrogen bonds [50] confirming the crosslinking between PVA by means of borax [51].

It is important to know the material's thermal stability to determine under what conditions it can be handled, stored, and sterilized. Therefore, the samples that met the criteria for injectability underwent TGA. As expected, the samples do not vary much from each other, since their composition is similar. **Error! Reference source not found.** (F) shows the result of the thermogravimetric evaluation from 25 ° to 1200 °C corresponding to F1, where the blue curve represents the TGA, and the orange one the DTG. The thermogram clearly identifies that the weight decreases with the increase in temperature, where 6 thermal events stand out. The first event around 100 °C with a weight loss of 5.5% attributed to the loss of moisture and volatile functional groups. This same event was reported by J. Barrera and co-authors, wherein their thermal analysis of PVA they found a percentage of surface water between 3 - 5% [52]. The PVA degradation process occurs in three steps [53]. The first occurs due to the degradation of the side chain of the polymer [54], in this case, it was identified around 225 °C with a weight loss of 2.81%. Then, at approximately 390 °C, the degradation of 26% of the material is identified, associated with the dehydration of the hydroxyl groups of the main chain of PVA [55]. Around 480 °C, a weight loss of 5.5 % occurs, which is attributed to the third stage of decomposition of PVA, where the C-C division of the main polymer chain occurs, called carbonation [56]. The localized processes after the one mentioned above, correspond to the degradation of proteins and fats of high molecular weight present in the demineralized bone matrix, in addition, it can be attributed to the loss of carbon dioxide, which was generated from the thermal decomposition of $CaCO_3$ in $CaO + CO_2$ [57]. Calcium oxide is the residual material in the sample, as it does not degrade at 1200 °C. Finally, the percentage of total weight loss was 84.5%, the residual percentage corresponds to possible phosphates present in the DBM and calcium oxides of $CaCO_3$ [58].

3.3. Degradation

The rate of degradation is one of the most important indicators to evaluate the quality of scaffolds since too fast or too slow degradation will seriously affect the application of the

Preprints (www.preprints.org) | NOT PEER-REVIEWED | Posted: 22 June 2021 doi:10.20944/preprints202106.0545.v1

scaffold [59]. **Error! Reference source not found.** shows the weight loss of F1 and F2 concerning the immersion time in days.

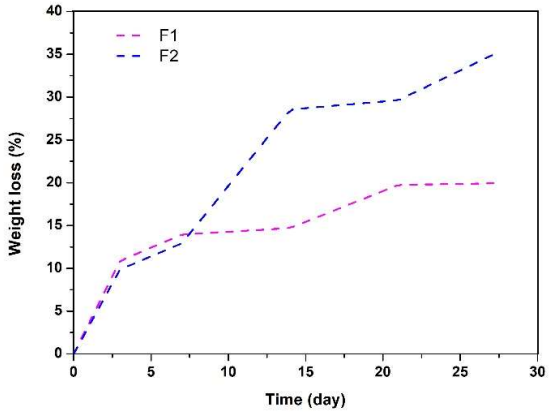

Figure 5. Degradation kinetics of the two formulations evaluated.

F2 lost about 35% of its weight after 28 days of immersion, and the rapid degradation of the material is an unfavorable aspect concerning the application that this research seeks. However, F1 had lost only 20% of its weight after 28 days of immersion, concluding that it is more stable compared to F2. Finally, when all the samples were weighed, the pH was also measured, that is, on days 3, 7, 14, 21, and 28. The results showed that until the end of the experiment, there were no significant differences in the values, given that all the formulations (at all times) maintained the pH of the fluid at 7.4 ± 0.2.

2.4. Bioactivity evaluation

The suitability of the present composite was examined by immersion in SBF for two weeks, followed by the analysis of the resulting surface layer by SEM-EDS. In **Error! Reference source not found.** the SEM micrographs of the two formulations that meet the injectability criteria are shown, before their immersion in SBF.

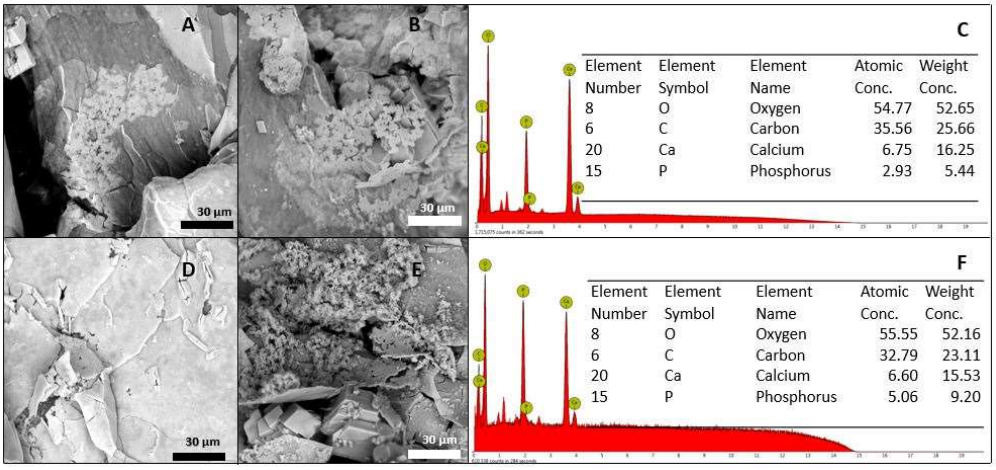

Figure 6. Bioactivity evaluation after 7 days of immersion (A) F1, (B) F2, and (C) EDS. Bioactivity evaluation after 14 days of immersion (D) F1, (E) F2, and (F) EDS.

After 7 days of immersion in SBF, the surface of these samples showed significant changes. In **Error! Reference source not found.**, the beginning of the formation of calcium

Preprints (www.preprints.org) | NOT PEER-REVIEWED | Posted: 22 June 2021 doi:10.20944/preprints202106.0545.v1

phosphate clusters is observed, whose Ca/P ratio was determined by EDS and was found in a range between 2.3 and 2.9 approx. The calcium/phosphorus ratio of apatite is reported between 1.5 and 2.6 [60], however, the evaluated formulations showed a layer formation of calcium phosphates with a slightly higher Ca/P ratio. This increase in the Ca/P ratio of the samples, compared to those reported in the literature, could be explained by the presence of calcium ions contributed by $CaCO_3$. After 14 days, the apatite clusters were able to deposit more uniformly, forming a predominant layer on the surface of the material, and reaching an approximate Ca/P ratio of 1.30, which is compared to the Ca/P ratio of amorphous calcium phosphates present in natural bone [61]**.** formulations (at all times) maintained the pH of the fluid at 7.4 ± 0.2.

2.5. MTT assay

The possible cytotoxic effect of demineralized bone matrix and the two injectable formulations developed in this work was evaluated using the MTT test, a colorimetric method that quantifies the activity of Succinic Dehydrogenase (SDH) [62], and is widely used as an indication of cellular mitochondrial function [63]. The results are shown in **Error! Reference source not found.**(A). For each treatment, the extract was tested at 100% and also its dilution at 50% in fresh medium. The absorbance values at 570 nm were analyzed by ANOVA and a post hoc test (Tukey's test). The statistical analysis of all treatments and the control, resulted in a p value > 0.05 by ANOVA, which denotes rejection of the null hypothesis that presumes equality of variances. The Tukey grouping with a confidence level of 95%, in the results of the extracts at 100%, showed that formulation 2 is significantly different from the control and the other treatments. However, in all cases the cell viability was higher than 70%, consequently, it is concluded that none of the materials generated a cytotoxic effect on the osteoblasts, even with the 100% extract.

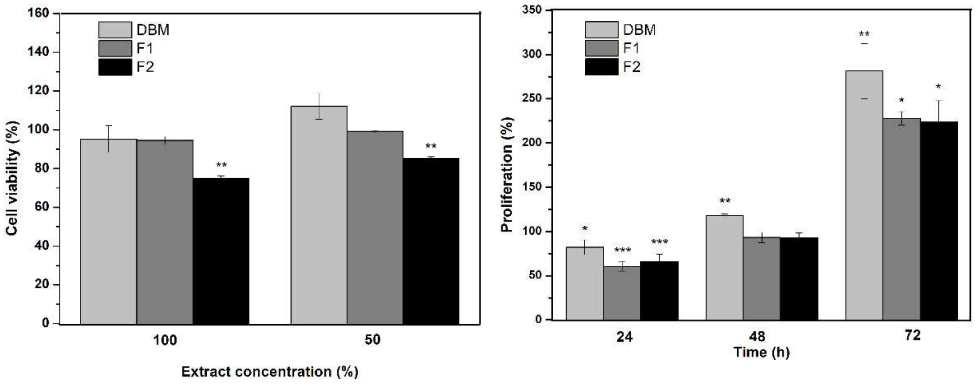

Figure 7. (A) Results of the MTT evaluation in percentage of cell viability. (B) Cell proliferation results. * p <0.05, ** p <0.01 and *** p ≤ 0.001 compared to the control. Error bars represent ± standard deviation.

2.6. Cell proliferation

The proliferation of Saos-2 osteoblasts treated with DBM and the injectable formulations were evaluated by quantifying the metabolic activity using the Alamar Blue kit at 24, 48, and 72 hours of incubation. The results are shown in
Figure 7(B) where the Y-axis represents the percentage of cell proliferation and the X-axis that of incubation in hours. At 24 hours, a lag phase in the culture was identified, since all the treatments significantly reduced cell viability. This event was attributed to cell adaptation [64] because proliferation was later evidenced, that is, the increase in cell viability as the incubation period was longer and compared to the control in each period of time.

 doi:10.20944/preprints202106.0545.v1

These results support those obtained by MTT, where none of the formulations were shown to have a cytotoxic effect on cells.

4. Discussion

Neves and co-authors indicate that for a bone substitute to be considered injectable, the force to extrude it through a syringe must be less than 100 N [65]. Under this criterion it is possible to conclude that with the exception of Formulation 3, all the formulations evaluated are injectable and whose injectability is greater than 90%. The percentages of injectability of these two formulations, when compared with those reported by Dorati and his collaborators, are high. They reported an injectable material, with an injectability between 70 and 75% and considered it acceptable for this type of application [66].

The formulations referred to in this work as Formulation 1 and Formulation 2 showed ease to be extruded by a syringe, which is a great advantage in minimally invasive surgeries, which reduce the risks of infections in the patient, decrease the time of the intervention and facilitate implantation to the surgeon [67]. IBS can be used to treat bone defects and/or irregularly shaped fractures because it can take its exact shape. This means that they can have closer or direct contact with the entire surface of the tissue to be treated, and also avoids the complications of block or preform grafts, which frequently present necrosis and mucosal perforation [68]. In addition, when the material is injected, it is not wasted because it enters to directly fill the bone defect. Formulation 3 presented an injectability of 59% ± 19, showing its low homogeneity at the time of injection, the force necessary to overcome the hydraulic pressure inside the syringe exceeds 100N, and this varies with the displacement. This could be explained by a phenomenon reported in the literature known as phase separation in injectable materials [69]. This fact occurs more frequently in injectables that have an aqueous phase, where a part of this can lodge near the needle with some precipitated solids, which generates a greater initial resistance to injection and then the material in the body of the syringe is a less homogeneous [70]. Therefore, this research continued evaluating Formulation 1 (F1) and Formulation 2 (F2).

A scaffold cannot provide appropriate microenvironments to protect cell proliferation and differentiation if the rate of degradation is too rapid. A slower rate of degradation can cause the scaffold residue to become foreign tissue or even induce an inflammatory response that will make it difficult to repair the bone defect site [71]. With this, it could be concluded that F1 compared to F2 would be the most appropriate to be used in bone regeneration, due to its structural stability and controlled degradation rate. Ziting bao et al. manufactured a Pluronic diacrylate hydrogel F127 (F127-da) and incorporated nano-$CaCO_3$ to improve bone regeneration, the results in the degradation test showed that the weight loss of the hydrogel decreased by approximately 15%. By incorporating calcium carbonate, and after 40 days of immersion in PBS, the hydrogel maintained approximately 85% of its mass, which, according to the authors, is beneficial in supporting bone tissue in its regeneration [7]. The pH remained balanced during the immersion time, this is attributed to the presence of $CaCO_3$, which has been widely reported and implemented to neutralize pH in degradation processes [72]. Furthermore, calcium carbonate improves cellular reaction relative to pure polymer, since it is a source of calcium ions that promote bone regeneration [73].

Bioactivity is the ability of a material to interact chemically with the living tissues of the body, this ability results from the release of ions until the formation of a mineralized layer on the surface of the material [74]. Bioactive materials must be able to form hydroxyapatite (HA) on their surface during immersion in SBF [75]. HA formation on the implant surface is considered the key factor for the creation of bone junction and the index of bone-forming capacity [76]. Both formulations evaluated showed the formation of calcium phosphates on their surfaces after immersion in SBF, therefore, qualitatively, it can be

 doi:10.20944/preprints202106.0545.v1

suggested that when the DBM is conveyed, in the polymeric and viscoelastic system developed, the bioactivity properties are not affected, and that the prototype of the injectable bone substitute obtained also has the ability to be bioactive, when in contact with simulated body fluid (SBF). These are formed from the free calcium ions, which bind with the phosphate ions in the SBF solution and then precipitate again at the active sites on the surface of the material. This demonstrates the capacity for biomineralization, which is an essential factor in promoting osteogenic bone-binding capacity for bone repair materials [34]. The calcium phosphates present in materials can cause bone induction through their high capacity to bind proteins (including growth factors), through their specific architectures, or the calcification of the living surface. For this reason, calcium phosphates ($Ca_3(PO_4)_2$) are widely used in bone repair and regeneration due to their osteoconductive and bioactive nature (osteointegration) [77].

In the case of the demineralized bone matrix, this proliferative effect was expected in human osteoblasts since DBM is composed of collagen and bone morphogenetic proteins. While the collagen matrix provides an osteoconductive effect, the BMPs provide osteoinductivity [78][79]. These results are consistent with those reported by Adkisson and his co-authors, who reported that human Saos-2 osteosarcoma cells proliferate in response to DBM [80]. Furthermore, they quantitatively correlated this proliferative activity with the osteoinductive capacity *in vivo*, however, this correlation was not significant [81] [82]. Jordan M. Katz and his collaborators also made efforts to determine the correlation of specific growth factors and cell proliferation in vitro versus ectopic bone formation in vivo. They found a significant positive correlation, but not sufficient to extrapolate the in vitro results with those obtained *in vivo* [83]. It should be noted that osteoinduction refers to the ability of a material to stimulate the differentiation of a cell towards a lineage of osteoblasts that will deposit minerals [84]. The high expression of alkaline phosphatase (ALP) is an early indicator of the differentiation and maturation of osteoblasts [85] and is one of the most reported forms of evaluation of in vitro osteoinduction [86]. Based on the above, we can conclude that when DBM is carried in the carrier polymeric system developed in this work, its proliferative capacity in human osteoblasts is not affected. It could also be suggested that the injectable material developed in this research has great potential to be an osteoinductive bone substitute, however, to conclude osteoinduction *in vitro*, quantitative bone differentiation tests such as ALP and semi-quantitative tests such as red staining should be performed. of alizarin [87] [88].

5. Conclusions

In this research, a polymeric system was developed to carry DBM and be used as an injectable bone substitute, which promises regenerative characteristics of bone tissue. The injectability test showed that two formulations capable of being extruded by a needleless syringe were developed, with a compression force of less than 100 N. It was also found that the injectability of both formulations was greater than 90%. The developed material is microporous with a porosity of around 50% that could favor protein adsorption and nutrient transport processes. When immersing the samples in simulated body fluid (SBF) and determining the degradation of the formulations, it was established that F1 was the one with the highest cohesion, that is, it was the one that showed less particle loss and greater stability in contact with the fluid. This formulation degraded by approx. 20%. after spending 28 days submerged in SBF. It was also found that none of the formulations altered the pH of the SBF during the time of the experiment. From the evaluation of the bioactivity, it can be determined that the IBS developed is a bioactive material, since all of the formulations evaluated promote the formation of calcium phosphates on the surface of the material. This means that the bioactive capacity of the DBM is not affected when it is integrated into the carrier system. By quantifying the mitochondrial activity of osteoblasts treated with DBM and injectable formulations using the MTT assay, it could be concluded that none of these materials induce cytotoxicity in cells. The results of the

quantification of the metabolic activity of osteoblasts using the Alamar Blue kit showed that when DBM is carried in the developed carrier system, its proliferative property in osteoblasts is not affected. Furthermore, this proliferative effect of injectable formulations suggests that these materials are osteoinductive, however, more evidence is needed to conclude it, for example, by quantifying markers of differentiation in osteoblasts and biomineralization.

Supplementary Materials: The following are available online at www.mdpi.com/xxx/s1, Figure S1: title, Table S1: title, Video S1: title.

Author Contributions: Daniela Medrano-David: Conceptualization, Methodology, Formal analysis, Investigation, Writing - original draft, Visualization; **A.M. Lopera-Echavarría:** Investigation, Writing-review & editing; **Martha E. Londoño:** Resources, Writing-review & editing, Funding acquisition, Project administration; **Pedronel Araque-Marín:** Conceptualization, Methodology, Writing-review & editing, Visualization, Supervision.

Funding: This research and the APC were funded by COLCIENCIAS, grant number 133377757790.

Acknowledgments: The authors wish to thank the COLCIENCIAS, EIA University, and Tissue Bank Foundation (Medellín, Colombia) for making this research possible.

Conflicts of Interest: The authors declare no conflict of interest. The funders had no role in the design of the study; in the collection, analyses, or interpretation of data; in the writing of the manuscript, or in the decision to publish the results.

References

[1] J. I. González Ocampo, M. M. Machado de Paula, N. J. Bassous, A. O. Lobo, C. P. Ossa Orozco, and T. J. Webster, "Osteoblast responses to injectable bone substitutes of kappa-carrageenan and nano hydroxyapatite," *Acta Biomater.*, vol. 83, pp. 425–434, Jan. 2019, doi: 10.1016/j.actbio.2018.10.023.

[2] Y. Li, J. Rodrigues, and H. Tomás, "Injectable and biodegradable hydrogels: Gelation, biodegradation and biomedical applications," *Chem. Soc. Rev.*, vol. 41, no. 6, pp. 2193–2221, 2012, doi: 10.1039/c1cs15203c.

[3] J. D. Kretlow, L. Klouda, and A. G. Mikos, "Injectable matrices and scaffolds for drug delivery in tissue engineering," *Adv. Drug Deliv. Rev.*, vol. 59, no. 4–5, pp. 263–273, 2007, doi: 10.1016/j.addr.2007.03.013.

[4] L. Wang *et al.*, "Application of injectable silk fibroin/graphene oxide hydrogel combined with bone marrow mesenchymal stem cells in bone tissue engineering," 2020, doi: 10.1016/j.colsurfa.2020.125318.

[5] K. Ren, H. Cui, Q. Xu, C. He, G. Li, and X. Chen, "Injectable Polypeptide Hydrogels with Tunable Microenvironment for 3D Spreading and Chondrogenic Differentiation of Bone-Marrow-Derived Mesenchymal Stem Cells," *Biomacromolecules*, vol. 17, no. 12, pp. 3862–3871, Dec. 2016, doi: 10.1021/acs.biomac.6b00884.

[6] F. Re *et al.*, "3D gelatin-chitosan hybrid hydrogels combined with human platelet lysate highly support human mesenchymal stem cell proliferation and osteogenic differentiation," *J. Tissue Eng.*, vol. 10, pp. 1–16, 2019, doi: 10.1177/2041731419845852.

[7] Z. Bao, Z. Gu, J. Xu, M. Zhao, G. Liu, and J. Wu, "Acid-responsive composite hydrogel platform with space-controllable stiffness and calcium supply for enhanced bone regeneration," *Chem. Eng. J.*, vol. 396, 2020, doi: 10.1016/j.cej.2020.125353.

[8] D. Vukajlovic, J. Parker, O. Bretcanu, and K. Novakovic, "Chitosan based polymer/bioglass composites for tissue engineering applications," 2018, doi: 10.1016/j.msec.2018.12.026.

[9] M. N. Sundaram, S. Amirthalingam, U. Mony, P. K. Varma, and R. Jayakumar, "Injectable chitosan-nano bioglass composite

hemostatic hydrogel for effective bleeding control," *Int. J. Biol. Macromol.*, vol. 129, pp. 936–943, 2019, doi: 10.1016/j.ijbiomac.2019.01.220.

[10] A. Mohebali, M. Abdouss, and F. Afshar Taromi, "Fabrication of biocompatible antibacterial nanowafers based on HNT/PVA nanocomposites loaded with minocycline for burn wound dressing," *Mater. Sci. Eng. C*, vol. 110, p. 110685, May 2020, doi: 10.1016/j.msec.2020.110685.

[11] S. Batool, Z. Hussain, M. B. K. Niazi, U. Liaqat, and M. Afzal, "Biogenic synthesis of silver nanoparticles and evaluation of physical and antimicrobial properties of Ag/PVA/starch nanocomposites hydrogel membranes for wound dressing application," *J. Drug Deliv. Sci. Technol.*, vol. 52, pp. 403–414, Aug. 2019, doi: 10.1016/j.jddst.2019.05.016.

[12] P. Das *et al.*, "Surface modification of electrospun PVA/chitosan nanofibers by dielectric barrier discharge plasma at atmospheric pressure and studies of their mechanical properties and biocompatibility," *Int. J. Biol. Macromol.*, vol. 114, pp. 1026–1032, Jul. 2018, doi: 10.1016/j.ijbiomac.2018.03.115.

[13] J. Ai, K. Li, J. Li, F. Yu, and J. Ma, "Super flexible, fatigue resistant, self-healing PVA/xylan/borax hydrogel with dual-crosslinked network," *Int. J. Biol. Macromol.*, vol. 172, pp. 66–73, 2021, doi: 10.1016/j.ijbiomac.2021.01.038.

[14] K. Koga, A. Takada, and N. Nemoto, "Dynamic light scattering and dynamic viscoelasticity of poly(vinyl alcohol) in aqueous borax solutions. 5. Temperature effects," *Macromolecules*, vol. 32, no. 26, pp. 8872–8879, Dec. 1999, doi: 10.1021/ma990493w.

[15] H. F. Mahjoub, M. Zammali, C. Abbes, and T. Othman, "Microrheological study of PVA/borax physical gels: Effect of chain length and elastic reinforcement by sodium hydroxide addition," *J. Mol. Liq.*, vol. 291, 2019, doi: 10.1016/j.molliq.2019.111272.

[16] J. Li, Y. Liu, and Q. Chen, "Conformation of dilute poly(vinyl alcohol)-borax complex by asymmetric flow field-flow fractionation," *J. Chromatogr. A*, vol. 1624, p. 461260, 2020, doi: 10.1016/j.chroma.2020.461260.

[17] H.-L. Lin, Y.-F. Liu, T. L. Yu, W.-H. Liu, and S.-P. Rwei, "Light scattering and viscoelasticity study of poly(vinyl alcohol)-borax aqueous solutions and gels," 2005, doi: 10.1016/j.polymer.2005.04.074.

[18] C. Zhao *et al.*, "A pH-Triggered, Self-Assembled, and Bioprintable Hybrid Hydrogel Scaffold for Mesenchymal Stem Cell Based Bone Tissue Engineering," *ACS Appl. Mater. Interfaces*, vol. 11, p. 51, 2019, doi: 10.1021/acsami.8b19094.

[19] Y. Liang, X. Zhao, P. X. Ma, B. Guo, Y. Du, and X. Han, "pH-responsive injectable hydrogels with mucosal adhesiveness based on chitosan-grafted-dihydrocaffeic acid and oxidized pullulan for localized drug delivery," *J. Colloid Interface Sci.*, vol. 536, pp. 224–234, Feb. 2019, doi: 10.1016/j.jcis.2018.10.056.

[20] P. J. Kondiah *et al.*, "A Review of Injectable Polymeric Hydrogel Systems for Application in Bone Tissue Engineering.," *Molecules*, vol. 21, no. 11, Nov. 2016, doi: 10.3390/molecules21111580.

[21] A. S. Hoffman, "Hydrogels for biomedical applications," *Advanced Drug Delivery Reviews*, vol. 64, no. SUPPL. Elsevier, pp. 18–23, Dec. 01, 2012, doi: 10.1016/j.addr.2012.09.010.

[22] M. Tian, Z. Yang, K. Kuwahara, M. E. Nimni, C. Wan, and B. Han, "Delivery of demineralized bone matrix powder using a thermogelling chitosan carrier," *Acta Biomater.*, vol. 8, no. 2, pp. 753–762, Feb. 2012, doi: 10.1016/j.actbio.2011.10.030.

[23] H. Kobayashi *et al.*, "Collagen immobilized PVA hydrogel-hydroxyapatite composites prepared by kneading methods as a

material for peripheral cuff of artificial cornea," in *Materials Science and Engineering C*, Dec. 2004, vol. 24, no. 6-8 SPEC. ISS., pp. 729–735, doi: 10.1016/j.msec.2004.08.038.

[24] N. Hameed, V. Glattauer, and J. A. M. Ramshaw, "Evaluation of polyvinyl alcohol composite membranes containing collagen and bone particles," *J. Mech. Behav. Biomed. Mater.*, vol. 48, pp. 38–45, Aug. 2015, doi: 10.1016/j.jmbbm.2015.04.005.

[25] L. A. Kinard *et al.*, "Synthetic biodegradable hydrogel delivery of demineralized bone matrix for bone augmentation in a rat model," *Acta Biomater.*, vol. 10, no. 11, pp. 4574–4582, Nov. 2014, doi: 10.1016/j.actbio.2014.07.011.

[26] S. M. Dizaj, M. Barzegar-Jalali, M. H. Zarrintan, K. Adibkia, and F. Lotfipour, "Calcium Carbonate Nanoparticles; Potential in Bone and Tooth Disorders," 2015. [Online]. Available: http://journals.tbzmed.ac.ir/PHARM.

[27] F. He, J. Zhang, F. Yang, J. Zhu, X. Tian, and X. Chen, "In vitro degradation and cell response of calcium carbonate composite ceramic in comparison with other synthetic bone substitute materials," 2015, doi: 10.1016/j.msec.2015.02.019.

[28] D. Eglin, D. Mortisen, and M. Alini, "Degradation of synthetic polymeric scaffolds for bone and cartilage tissue repairs," *Soft Matter*, vol. 5, no. 5, pp. 938–947, Feb. 2009, doi: 10.1039/b803718n.

[29] D. Hikmawati, H. N. Maulida, A. P. Putra, A. S. Budiatin, and A. Syahrom, "Synthesis and Characterization of Nanohydroxyapatite-Gelatin Composite with Streptomycin as Antituberculosis Injectable Bone Substitute," *Int. J. Biomater.*, vol. 2019, 2019, doi: 10.1155/2019/7179243.

[30] R. Mishra, R. Varshney, N. Das, D. Sircar, and P. Roy, "Synthesis and characterization of gelatin-PVP polymer composite scaffold for potential application in bone tissue engineering," *Eur. Polym. J.*, vol. 119, pp. 155–168, 2019, doi: 10.1016/j.eurpolymj.2019.07.007.

[31] T. Kokubo and H. Takadama, "How useful is SBF in predicting in vivo bone bioactivity?," *Biomaterials*, vol. 27, no. 15, pp. 2907–2915, May 2006, doi: 10.1016/j.biomaterials.2006.01.017.

[32] Z. Yang *et al.*, "Degradable photothermal bioactive glass composite hydrogel for the sequential treatment of tumor-related bone defects: From anti-tumor to repairing bone defects," *Chem. Eng. J.*, vol. 419, p. 129520, 2021, doi: 10.1016/j.cej.2021.129520.

[33] X. Jing *et al.*, "Morphology, mechanical properties, and shape memory effects of poly(lactic acid)/ thermoplastic polyurethane blend scaffolds prepared by thermally induced phase separation," *J. Cell. Plast.*, vol. 50, no. 4, pp. 361–379, 2014, doi: 10.1177/0021955X14525959.

[34] X. yun Zhang *et al.*, "Biocompatiable silk fibroin/carboxymethyl chitosan/strontium substituted hydroxyapatite/cellulose nanocrystal composite scaffolds for bone tissue engineering," *Int. J. Biol. Macromol.*, vol. 136, pp. 1247–1257, Sep. 2019, doi: 10.1016/j.ijbiomac.2019.06.172.

[35] A. Pal, B. L. Vernon, and M. Nikkhah, "Therapeutic neovascularization promoted by injectable hydrogels," *Bioactive Materials*, vol. 3, no. 4. KeAi Communications Co., pp. 389–400, Dec. 01, 2018, doi: 10.1016/j.bioactmat.2018.05.002.

[36] J. Zhang *et al.*, "A simple and effective approach to prepare injectable macroporous calcium phosphate cement for bone repair: Syringe-foaming using a viscous hydrophilic polymeric solution," *Acta Biomater.*, vol. 31, pp. 326–338, Feb. 2016, doi: 10.1016/j.actbio.2015.11.055.

[37] M. Bohner and G. Baroud, "Injectability of calcium phosphate pastes," *Biomaterials*, vol. 26, no. 13, pp. 1553–1563, May 2005, doi: 10.1016/j.biomaterials.2004.05.010.

[38] D. H. Shaw, "Drugs Acting on the Gastrointestinal Tract," in *Pharmacology and Therapeutics for Dentistry: Seventh Edition*, Elsevier, 2017, pp. 404–416.

[39] B. Oyeneyin, *Introduction to the Hydrocarbon Composite Production System*, vol. 63. 2015.

[40] A. A. Vu, D. A. Burke, A. Bandyopadhyay, and S. Bose, "Effects of surface area and topography on 3D printed tricalcium phosphate scaffolds for bone grafting applications," *Addit. Manuf.*, vol. 39, p. 101870, Mar. 2021, doi: 10.1016/j.addma.2021.101870.

[41] G. T. El-Bassyouni, O. W. Guirguis, and W. I. Abdel-Fattah, "Morphological and macrostructural studies of dog cranial bone demineralized with different acids," *Curr. Appl. Phys.*, vol. 13, no. 5, pp. 864–874, 2013, doi: 10.1016/j.cap.2012.12.026.

[42] R. Murugan, S. Ramakrishna, and K. Panduranga Rao, "Nanoporous hydroxy-carbonate apatite scaffold made of natural bone," *Mater. Lett.*, vol. 60, no. 23, pp. 2844–2847, 2006, doi: 10.1016/j.matlet.2006.01.104.

[43] S. I. Qashou, E. F. M. El-Zaidia, A. A. A. Darwish, and T. A. Hanafy, "Methylsilicon phthalocyanine hydroxide doped PVA films for optoelectronic applications: FTIR spectroscopy, electrical conductivity, linear and nonlinear optical studies," *Phys. B Condens. Matter*, vol. 571, pp. 93–100, 2019, doi: 10.1016/j.physb.2019.06.063.

[44] N. A. Peppas, "Tear propagation resistance of semicrystalline polymeric networks," *Polymer (Guildf).*, vol. 18, no. 4, pp. 403–407, 1977, doi: 10.1016/0032-3861(77)90090-8.

[45] C. M. Hassan and N. A. Peppas, "Structure and applications of poly(vinyl alcohol) hydrogels produced by conventional crosslinking or by freezing/thawing methods," *Advances in Polymer Science*, vol. 153. Springer New York, pp. 37–65, 2000, doi: 10.1007/3-540-46414-x_2.

[46] J. Thomas, A. Lowman, and M. Marcolongo, "Novel associated hydrogels for nucleus pulposus replacement," *J. Biomed. Mater. Res. - Part A*, vol. 67, no. 4, pp. 1329–1337, 2003, doi: 10.1002/jbm.a.10119.

[47] W. E. Hennink and C. F. Van Nostrum, "Novel crosslinking methods to design hydrogels," *Adv. Drug Deliv. Rev.*, vol. 54, no. 1, pp. 13–36, Jan. 2002, doi: 10.1016/S0169-409X(01)00240-X.

[48] Y. Ma, T. Bai, and F. Wang, "The physical and chemical properties of the polyvinylalcohol/polyvinylpyrrolidone/hydroxyapatite composite hydrogel," *Mater. Sci. Eng. C*, vol. 59, pp. 948–957, Feb. 2016, doi: 10.1016/j.msec.2015.10.081.

[49] J. P. Harrison and D. Berry, "Vibrational spectroscopy for imaging single microbial cells in complex biological samples," *Frontiers in Microbiology*, vol. 8, no. APR. Frontiers Media S.A., Apr. 13, 2017, doi: 10.3389/fmicb.2017.00675.

[50] M. Kobayashi, Y. Kitaoka, and M. Kobayashi, "Complex formation of boric acids with DI- and TRI- carboxylic acids and poly(vinyl alcohol) in aqueous solutions," *Macromol. Symp.*, vol. 114, no. 1, pp. 303–308, Feb. 1997, doi: 10.1002/masy.19971140141.

[51] M. Huang, Y. Hou, Y. Li, D. Wang, and L. Zhang, "High performances of dual network PVA hydrogel modified by PVP

using borax as the structure-forming accelerator," *Des. Monomers Polym.*, vol. 20, no. 1, pp. 505–513, 2017, doi: 10.1080/15685551.2017.1382433.

[52] N. Barrera, J., Rodríguez, J., Perilla, J., Algecira, "Estudio de la degradación térmica de poli(alcohol vinílico) mediante termogravimetría y termogravimetría diferencial," *Ing Investig , pp. 100 - 105*, 2007. https://www.scopus.com/record/display.uri?eid=2-s2.0-84887494116&origin=inward&txGid=4a7491656262c8f2ee6a5b7748c813a6 (accessed Nov. 22, 2020).

[53] M. Premalatha, N. Vijaya, S. Selvasekarapandian, and S. Selvalakshmi, "Characterization of blend polymer PVA-PVP complexed with ammonium thiocyanate," *Ionics (Kiel).*, vol. 22, no. 8, pp. 1299–1310, Aug. 2016, doi: 10.1007/s11581-016-1672-7.

[54] J. Wang, C. Gao, Y. Zhang, and Y. Wan, "Preparation and in vitro characterization of BC/PVA hydrogel composite for its potential use as artificial cornea biomaterial," *Mater. Sci. Eng. C*, vol. 30, no. 1, pp. 214–218, 2010, doi: 10.1016/j.msec.2009.10.006.

[55] S. K. Tripathi, A. Gupta, and M. Kumari, "Dielectric and Modulus spectra (Bode) _____Studies on electrical conductivity and dielectric behaviour of PVdF–HFP–PMMA–NaI polymer blend electrolyte," *Bull. Mater. Sci.*, vol. 35, no. 6, pp. 969–975, 2012, [Online]. Available: http://link.springer.com/10.1007/s12034-012-0387-2.

[56] C. C. Yang *et al.*, "Preparation of a PVA/HAP composite polymer membrane for a direct ethanol fuel cell (DEFC)," *J. Appl. Electrochem.*, vol. 38, no. 10, pp. 1329–1337, Oct. 2008, doi: 10.1007/s10800-008-9563-x.

[57] S. Sun, D. Gebauer, and H. Cölfen, "A solvothermal method for synthesizing monolayer protected amorphous calcium carbonate clusters," *Chem. Commun.*, vol. 52, no. 43, pp. 7036–7038, May 2016, doi: 10.1039/c6cc03010f.

[58] L. Li, Y. Yang, Y. Lv, P. Yin, and T. Lei, "Porous calcite CaCO3 microspheres: Preparation, characterization and release behavior as doxorubicin carrier," *Colloids Surfaces B Biointerfaces*, vol. 186, p. 110720, Feb. 2020, doi: 10.1016/j.colsurfb.2019.110720.

[59] T. M. Freyman, I. V. Yannas, and L. J. Gibson, "Cellular materials as porous scaffolds for tissue engineering," *Progress in Materials Science*, vol. 46, no. 3–4. Pergamon, pp. 273–282, Jan. 01, 2001, doi: 10.1016/S0079-6425(00)00018-9.

[60] S. Minagar, J. Lin, Y. Li, C. C. Berndt, and C. Wen, "Nanotopography and surface chemistry of TiO2-ZrO2-ZrTiO4 nanotubular surfaces and the influence on their bioactivity and cell responses," in *Metallic Foam Bone: Processing, Modification and Characterization and Properties*, Woodhead Publishing, 2017, pp. 181–202.

[61] F. De Odontología *et al.*, "UNIVERSIDAD COMPLUTENSE DE MADRID TESIS DOCTORAL Un composite nuevo de fosfato cálcico-silicato cálcico para la regeneración ósea: caracterización y comportamiento MEMORIA PARA OPTAR AL GRADO DE DOCTOR PRESENTADA POR," 2014.

[62] Y. Rai *et al.*, "Mitochondrial biogenesis and metabolic hyperactivation limits the application of MTT assay in the estimation of radiation induced growth inhibition," *Sci. Rep.*, vol. 8, no. 1, Dec. 2018, doi: 10.1038/s41598-018-19930-w.

[63] M. Parmaksiz, Ö. Lalegül-Ülker, M. T. Vurat, A. E. Elçin, and Y. M. Elçin, "Magneto-sensitive decellularized bone matrix with or without low frequency-pulsed electromagnetic field exposure for the healing of a critical-size bone defect," *Mater.*

Sci. Eng. C, vol. 124, p. 112065, May 2021, doi: 10.1016/j.msec.2021.112065.

[64] N. Dadgar *et al.*, "Cartilage tissue engineering using injectable functionalized Demineralized Bone Matrix scaffold with glucosamine in PVA carrier, cultured in microbioreactor prior to study in rabbit model," *Mater. Sci. Eng. C*, vol. 120, 2021, doi: 10.1016/j.msec.2020.111677.

[65] N. Neves *et al.*, "Strontium-rich injectable hybrid system for bone regeneration," *Mater. Sci. Eng. C*, vol. 59, pp. 818–827, Feb. 2016, doi: 10.1016/j.msec.2015.10.038.

[66] R. Dorati *et al.*, "In vitro characterization of an injectable in situ forming composite system for bone reconstruction," *Polym. Degrad. Stab.*, vol. 119, pp. 151–158, Jun. 2015, doi: 10.1016/j.polymdegradstab.2015.05.001.

[67] S. A. Bencherif *et al.*, "Injectable preformed scaffolds with shape-memory properties," *Proc. Natl. Acad. Sci. U. S. A.*, vol. 109, no. 48, pp. 19590–19595, Nov. 2012, doi: 10.1073/pnas.1211516109.

[68] V. V. Thai and B. T. Lee, "Fabrication of calcium phosphate-calcium sulfate injectable bone substitute using hydroxy-propyl-methyl-cellulose and citric acid," *J. Mater. Sci. Mater. Med.*, vol. 21, no. 6, pp. 1867–1874, Jun. 2010, doi: 10.1007/s10856-010-4058-9.

[69] R. O. Neill *et al.*, "Acta Biomaterialia Critical review : Injectability of calcium phosphate pastes and cements," *Acta Biomater.*, vol. 50, pp. 1–19, 2017, doi: 10.1016/j.actbio.2016.11.019.

[70] R. O'Neill *et al.*, "Critical review: Injectability of calcium phosphate pastes and cements," *Acta Biomaterialia*, vol. 50. Elsevier Ltd, pp. 1–19, Mar. 01, 2017, doi: 10.1016/j.actbio.2016.11.019.

[71] P. M. Mountziaris and A. G. Mikos, "Modulation of the inflammatory response for enhanced bone tissue regeneration," *Tissue Engineering - Part B: Reviews*, vol. 14, no. 2. Mary Ann Liebert, Inc. 140 Huguenot Street, 3rd Floor New Rochelle, NY 10801 USA, pp. 179–186, Jun. 10, 2008, doi: 10.1089/ten.teb.2008.0038.

[72] C. Schiller and M. Epple, "Carbonated calcium phosphates are suitable pH-stabilising fillers for biodegradable polyesters," *Biomaterials*, vol. 24, no. 12, pp. 2037–2043, May 2003, doi: 10.1016/S0142-9612(02)00634-8.

[73] R. Aquino-Martínez, N. Artigas, B. Gámez, J. L. Rosa, and F. Ventura, "Extracellular calcium promotes bone formation from bone marrow mesenchymal stem cells by amplifying the effects of BMP-2 on SMAD signalling," *PLoS One*, vol. 12, no. 5, p. e0178158, May 2017, doi: 10.1371/journal.pone.0178158.

[74] R. A. Alhashimi, F. Mannocci, and S. Sauro, "Bioactivity, cytocompatibility and thermal properties of experimental Bioglass-reinforced composites as potential root-canal filling materials," *J. Mech. Behav. Biomed. Mater.*, vol. 69, pp. 355–361, May 2017, doi: 10.1016/j.jmbbm.2017.01.022.

[75] R. Al-Wafi, S. S. Eldera, and E. M. A. Hamzawy, "Characterization and in vitro bioactivity study of a new glass ceramic from mica/apatite glass mixtures," *J. Mater. Res. Technol.*, vol. 9, no. 4, pp. 7558–7569, Jul. 2020, doi: 10.1016/j.jmrt.2020.05.074.

[76] S. R. Radin and P. Ducheyne, "The effect of calcium phosphate ceramic composition and structure on in vitro behavior. II. Precipitation," *J. Biomed. Mater. Res.*, vol. 27, no. 1, pp. 35–45, 1993, doi: 10.1002/jbm.820270106.

[77] H. Yuan, D. Barbieri, X. Luo, C. A. Van Blitterswijk, and J. D. De Bruijn, "Calcium phosphates and bone induction," *Compr.*

Biomater. II, vol. 1, no. October 2016, pp. 333–349, 2017, doi: 10.1016/B978-0-12-803581-8.10241-3.

[78] T. T. Roberts and A. J. Rosenbaum, "Bone grafts, bone substitutes and orthobiologics The bridge between basic science and clinical advancements in fracture healing," 2012, doi: 10.4161/org.23306.

[79] C. T. Laurencin and T. Jiang, *Bone Graft Substitutes and Bone Regenerative Engineering, 2nd Edition*. 2014.

[80] H. D. Adkisson, J. Strauss-Schoenberger, M. Gillis, R. Wilkins, M. Jackson, and K. A. Hruska, "Rapid quantitative bioassay of osteoinduction," *J. Orthop. Res.*, vol. 18, no. 3, pp. 503–511, 2000, doi: 10.1002/jor.1100180326.

[81] J. Glowacki, "A review of osteoinductive testing methods and sterilization processes for demineralized bone," *Cell Tissue Bank.*, vol. 6, no. 1, pp. 3–12, 2005, doi: 10.1007/s10561-005-4252-z.

[82] A. M. C. Barradas, H. Yuan, C. A. van Blitterswijk, and P. Habibovic, "Osteoinductive biomaterials: current knowledge of properties, experimental models and biological mechanisms.," *Eur. Cell. Mater.*, vol. 21, pp. 407–429, 2011, doi: 10.22203/eCM.v021a31.

[83] J. M. Katz, C. Nataraj, R. Jaw, E. Deigl, and P. Bursac, "Demineralized bone matrix as an osteoinductive biomaterial and in vitro predictors of its biological potential," *J. Biomed. Mater. Res. - Part B Appl. Biomater.*, vol. 89, no. 1, pp. 127–134, 2009, doi: 10.1002/jbm.b.31195.

[84] K. M. Pawelec, A. A. White, and S. M. Best, "Properties and characterization of bone repair materials," in *Bone Repair Biomaterials*, Elsevier, 2019, pp. 65–102.

[85] X. Zhao, M. Liang, X. Li, X. Qiu, and L. Cui, "Identification of key genes and pathways associated with osteogenic differentiation of adipose stem cells," *J. Cell. Physiol.*, vol. 233, no. 12, pp. 9777–9785, Dec. 2018, doi: 10.1002/jcp.26943.

[86] B. Han, B. Tang, and M. E. Nimni, "Quantitative and sensitive in vitro assay for osteoinductive activity of demineralized bone matrix," *J. Orthop. Res.*, vol. 21, no. 4, pp. 648–654, 2003, doi: 10.1016/S0736-0266(03)00005-6.

[87] M. Zhao *et al.*, "Evaluation of long-term biocompatibility and osteogenic differentiation of graphene nanosheet doped calcium phosphate-chitosan AZ91D composites," *Mater. Sci. Eng. C*, vol. 90, pp. 365–378, Sep. 2018, doi: 10.1016/j.msec.2018.04.082.

[88] Y. Wang, Y. Bian, L. Zhou, B. Feng, X. Weng, and R. Liang, "Biological evaluation of bone substitute," *Clinica Chimica Acta*, vol. 510. pp. 544–555, 2020, doi: 10.1016/j.cca.2020.08.017.